

This paper has been accepted for publication in the AEE journal. This is the version, which has not been fully edited and content may change prior to final publication.

Citation information: DOI 10.24425/ae.2026.1521

Adaptive sliding-mode control for robust PV power extraction under dynamic environmental conditions

SALISU ABDULLAHI*¹, KHALED ELTAG¹, CHEN XIAOHU¹, LEI WEINING¹,
KENT BERTILSSON²

¹*School of Mechanical and Electrical Engineering, Quanzhou University of Information Engineering
249 Bodong Road, Quanzhou, Fujian, China*

²*Department of Computer and Electrical Engineering, Mid Sweden University
851 70 Sundsvall, Sweden*

*e-mail: *salisuabdullahisaleh@gmail.com, khaledeltag@yahoo.com,
{chenxiaohu/leiweining}@qzuie.edu.cn, kent.bertilsson@miun.se*

Abstract: This paper proposes a robust sliding-mode control strategy for efficient photovoltaic (PV) energy extraction in island DC microgrids. A PV system is sensitive to voltage fluctuations. PV parameters are optimized, shunt resistance, saturation, reverse saturation, and photovoltaic current equations are modeled to maximize power generation. A boost converter increases PV output voltage to commercial levels, with the parameters carefully optimized for maximum performance. The converters are modeled using first-order differential equations based on an average state-space representation, enabling the development of a sliding-mode control strategy with non-linear switching functions. The control strategy incorporates reachability dynamics to handle system non-linearities, with the control law formulated using surface switching and equivalent control. This ensures precise regulation, fast convergence, and robust performance. Validated in MATLAB/Simulink under nominal (0.6 mH) and perturbed (0.9 mH) converter inductance conditions. The results reveal: (i) fast convergence with settling times of 2.0 ms under nominal and perturbed conditions; (iii) robust performance with 8.5% overshoots (nominal) and 10.0% overshoots (perturbed), compared to 26.0% and 33.0% with conventional PID controllers. As converter inductance parameters vary, the system achieves optimal power extraction. This study shows how sliding-mode control can enhance PV system performance for microgrid applications.

Keywords: boost power converter, islanded DC microgrid, MATLAB/Simulink, PV system, robust sliding-mode control

1. Introduction

The DC microgrid system (DCMS) has gained considerable prominence over the past few years in comparison to AC microgrid systems. The DCMS eliminates issues like contact problems, surge current issues, and nearby impacts since it operates without frequency. Furthermore, the DCMS is more compatible with photovoltaic (PV) integration [1–5]. Efficient

This paper has been accepted for publication in the AEE journal. This is the version, which has not been fully edited and content may change prior to final publication.
Citation information: DOI 10.24425/ae.2026.1521

study of PV systems necessitates a detailed understanding of the power distribution graphs of solar panels. The performance distribution graphs of solar panels were affected through external factors like irradiance and temperature at the installation site [6, 7]. Boost converters [8], particularly the widely used step-up converters, serve an essential part at maximizing energy conversion from PV applications, including DC microgrid control applications. Variable structure sliding-mode control involves a specific technique characterized by small-amplitude, high-frequency switching movements along a predefined trajectory. This method offers simplicity in the algorithm, high reliability, and robustness compared to other control strategies [9].

An idea for combining low-power, varying energy resources and controllable loads to create dynamic system referred to as microgrid systems (MSs) was developed earlier [10], potentially achieving more traceable control. An MS can be operated independently to a distribution network. Based on the PCC voltage configuration, the ACMS and DCMS can be distinguished [2]. ACMSs' performance has improved significantly over the past decade. Artificial intelligence, model predictive control, and hierarchical structures have recently been developed [11–18], however, boost converters are recognized as more attractive for changing the voltage level in DCMS applications as presented in Fig. 1 by their greater performance, better convenient connections to renewable energy resources, energy storage system, DC grid and higher compatibility compared to home devices standards. In the microgrid hierarchy, the proposed approach operates at the primary control level (millisecond time scale). It complements secondary control (voltage restoration, power balancing) and tertiary control (economic dispatch, energy management) for PV-boost converter systems. The proposed strategy handles fast transients, while higher-level controllers handle slower dynamics, enabling overall system stability and efficiency.

Further, control of energy systems has been developed across multiple time scales. In addition to coordinated optimization approaches for flexible load response [19], fuzzy logic, neural networks, and adaptive neuro-fuzzy inference systems-based PV control models [20], embedded microcontrollers for PID speed regulation [21] are also included.

Multilevel converters based on battery ESSs (BESSs) have been proposed in [22] that employ an optimization approach to energy management. However, their layered structure posed practical implementation challenges despite achieving their control objectives. This limitation was addressed in [23] by connecting a DC grid to BESSs via a two-way active converter. When applied to DC microgrids, this method has some limitations, despite its relative ease of construction. Microgrids rely on droop control to maintain a steady DC grid voltage by ensuring equal power distribution, as extensively discussed in references [24]. As a consequence of line impedance fluctuation problems generated via cable resistance, droop controllers may affect the efficiency of load power distribution. Controllers with fuzzy logic gain schedules were used to address this issue [25]. In addition, a method of fuzzy logic control was introduced to maintain the DC-bus voltage and balance load-to-generator power distribution. However, this approach lacks dynamical models in its design methodology, which makes it insufficient for representing the dynamics of the system. Furthermore, linearized models were typically used to design the

controllers mentioned above. Thus, they may not deliver desired control performance under changing conditions, as discussed in [26]. DC microgrids, on the other hand, are nonlinear and complex because of the presence of many converters. As a result, nonlinear control schemes are increasingly being explored in order to maintain reliable operation across a variety of operational circumstances.

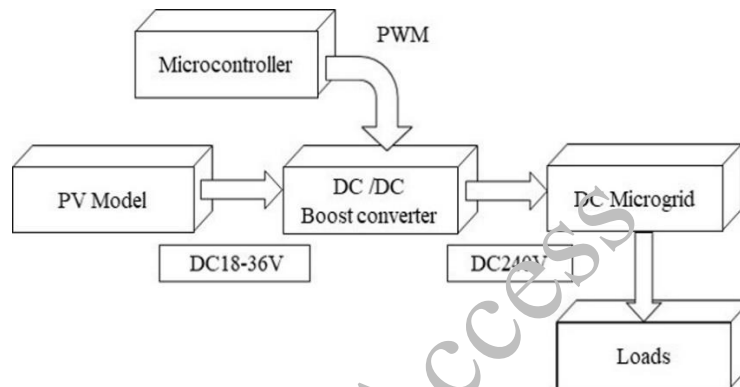


Fig. 1. Block diagram of a solar PV power converter system

Model predictive controllers (MPC) are widely used for minimizing cost functions and generating converter control signals [27]. To address the impact of pulse loads in DC/DC converters, [28] an MPC scheme was proposed. In [29], an MPC was introduced to improve the stability of DC/DC converters. Despite its practicality, there are several limitations to this control technique, including parameter accuracy and time-consuming optimization. For overcoming these problems, the non-linear feedback linearization controller (FBLC) has been recognized for DC microgrid applications. A FBLC approach was presented in [30] to maintain DC-bus voltage balance within DC microgrids while regulating DC-bus voltage. In addition, Reference [31] described an adaptive FBLC that predicts undisclosed parameters and ensures power distribution. The effectiveness of these control strategies is dependent on system factors. As operating conditions vary, it can be difficult to obtain accurate system parameter information in practical applications. Moreover, this control approach often ignores nonlinear factors that could improve transient stability. Consequently, switching to nonlinear backstepping control instead of FBLC schemes may improve transient responses in [32]. In [33], the stability of the hybrid DC microgrid dynamics was assessed using a nonlinear backstepping controller (BSC). Voltage control and power balance were successfully achieved based on simulation results. An adaptive BSC version was presented in [34], which improves the efficiency of power sharing thereby maintains DC grid voltage regulation under unknown conditions. As a result, there are practical limitations because the result of the control parameters must be taken repeatedly, especially for cases of high-level systems. Moreover, to achieve optimal efficiency, user-defined gain levels must be precisely tuned, creating another level of difficulty [35]. SMCs represent an effective

alternative to BSCs and FBLCs, as discussed in [36]. It was presented in [37] to use an ideal distributed energy resource system (DERS) to control power flow between DERS components and the DC grid for an islanded DC microgrid application. DC/DC power converters in DERSs have been proposed with a variety of second-order controllers, but existing studies [2–4, 8, 28–30] assume constant DER sources, ignoring the dynamic effects of environmental and PV parameter changes. Crucially, the real-world performance of PV dynamic equations for DCMS applications under varying conditions remains unexplored. Ultraviolet, visible, and near-infrared wavelengths are all absorbed by PV panels. Panels are heated by 50% of solar radiation in the infrared spectrum. We use radiometric quantities like irradiance (W/m²) throughout this study.

This research addresses this gap by:

1. **Developing a detailed mathematical model of the PV system** in order to maximize voltage output under different parametric and dynamic conditions.
2. **Proposing a sliding-mode control strategy** for a boost converter, integrating prior concepts while accounting for PV parameter uncertainties.
3. **Validating the control design** against real-world PV model variations—a critical step overlooked in the existing literature.

Unlike previous studies, our study rigorously tests the PV mathematical model within a control framework rather than focusing only on ideal PV output voltage. In DC microgrid applications, this ensures robustness against parametric uncertainties. This paper presents the design and implementation of a robust sliding-mode control (SMC) strategy to efficiently extract energy from photovoltaic (PV) systems for islanded DC microgrid applications. PV systems exhibit varying output voltages due to environmental factors such as irradiance and temperature. To maximize power generation, the PV system parameters—including saturation current, reverse saturation current, shunt resistance, and photovoltaic current—are optimized using precise mathematical equations. A DC/DC boost converter is employed to increase the PV system's output voltage to levels suitable for commercial applications. The converter is accurately designed to maximize power output and is modeled using first-order differential equations based on an average state-space approach. The proposed sliding-mode control strategy incorporates a nonlinear switching function to handle system nonlinearities, with the reach dynamic equation ensuring stability and convergence. The control law is formulated using equivalent control and surface switching control, which together optimize the system's performance. The rest of this paper is structured as follows: **Section 1** provides an overview of existing control strategies. **Section 2** discusses photovoltaic systems and power converter modeling. **Section 3** details the proposed controller design. **Section 4** presents and analyzes simulation results. Finally, **Section 5** concludes the paper with key findings and future research.

2. System modeling

In this section, we discuss the mathematical modeling of the photovoltaic system and the boost converter. A PV cell model is presented in **Section 2.1**, including the single-diode

equivalent circuit, photocurrent, saturation currents, and parasitic resistances (R_s and R_{sh}). Boost converter topology, operating modes, and component design equations for inductance (L) and capacitance (C) are discussed in **Section 2.2**.

2.1. Photovoltaic

Photovoltaic systems are composed of an individual diode linked in parallel with a radiation source, I_{ph} (Fig. 2(a)), whose electrical current I appears to be expressed as [6]:

$$I = I_{ph} - I_s \left[\exp\left(\frac{V}{nV_t}\right) - 1 \right], \quad (1)$$

where I_s is the current saturation, representing the minimal current pass through the diode under reverse bias. V is the PV voltage, the voltage across the photovoltaic cell. $V_t = kT_c/q$, represents the thermal voltage. k represents the constant Boltzmann, and is the relationship between temperature and energy in a semiconductor (1.38×10^{-23} J/K). T_c is the temperature of the photovoltaic cell that influences the output characteristic of the panels.

q = charge electron (1.6×10^{-19} C),

n = factor ideality (11/10).

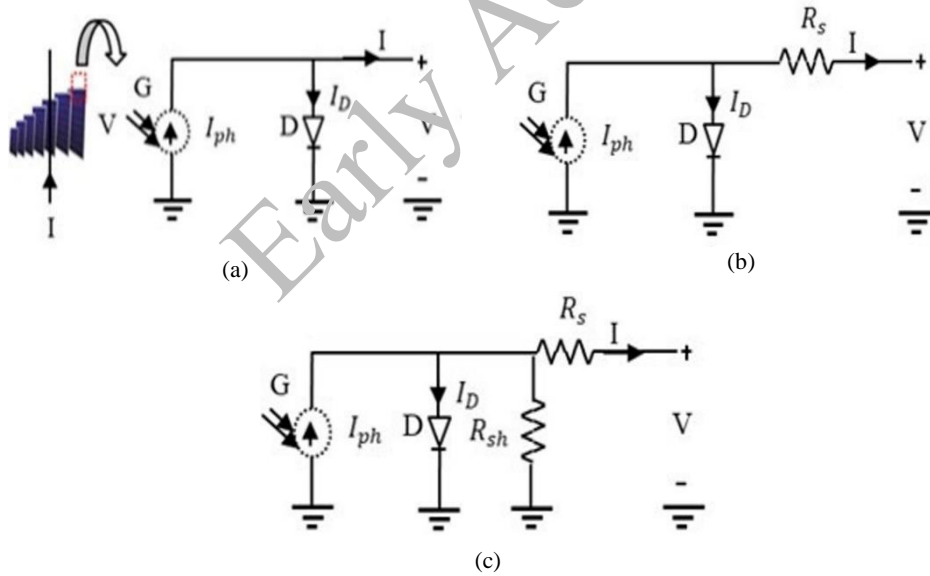


Fig. 2. Circuit solar PV cells: (a) none resistance connection; (b) resistance connection series, R_s ; (c) resistance connection series and parallel, R_s and R_{sh}

A non-ideal photovoltaic model with series resistance R_s is depicted in Fig. 2(b), the output current can be derived as:

$$I = I_{ph} - I_s \left[\exp\left(\frac{V+IR_s}{nV_t}\right) - 1 \right]. \quad (2)$$

Expression (2) could never accurately describe the performance of the cell when exposed to atmospheric changes, particularly at lower potentials. A photovoltaic system consisting of series and parallel resistances is presented as the most feasible scheme, as shown in (Fig. 2(c)), including parallel resistances R_{sh} and series resistances R_s [6]. Due to the ohmic contact between the metal and semiconductor, R_s is very small. However, R_{sh} is extremely high and shows the level of quality along the boundary (remark: in a perfect situation, $R_s = 0$ and R_{sh} is infinity [7]).

By using the Kirchhoff equation at this junction I_{ph} , I_D , R_{sh} and R_s as shown in Fig. 2(c), the expression could be presented as follows:

$$I = I_{ph} - I_D - I_{sh}, \quad (3)$$

$$I = I_{ph} - I_s \left[\exp\left(\frac{V+IR_s}{nV_t}\right) - 1 \right] - \frac{V+IR_s}{R_{sh}}. \quad (4)$$

I_D represents the diode (D) current, I_{sh} represents the shunt current, and G represents the solar irradiation.

To provide clarity, the simple diode representation in Fig. 2(c) has been employed during the current research work. The photocurrent mainly depends on the insolation and cell's working temperature, which is described as [6]:

$$I_{ph} = [1 + K_I(T_c - T_{ref})] \frac{G}{G_{ref}}, \quad (5)$$

where: I_{sc} is the current solar cell, G_{ref} is the insolation reference, T_{ref} represents the cell's reference temperature, K_I stands for the coefficient temperature, and G is the insolation.

The saturation current is presented below:

$$I_s = I_{RS} \left(\frac{T_c}{T_{ref}}\right)^3 \exp\left[\frac{qE_g}{nk} \left(\frac{1}{T_{ref}} - \frac{1}{T_c}\right)\right], \quad (6)$$

where: I_{RS} is the current reverse saturation, E_g is the solar cell band-gap energy, and n is the PV dependent.

The current reverse saturation is given below:

$$I_{RS} = \frac{I_{sc}}{\exp\left(\frac{qV_{oc}}{nkT_c}\right) - 1}. \quad (7)$$

2.2. Boost converter

When the input voltage is less than the output voltage, a boost DC/DC power converter can increase the output voltage. A boost DC/DC power converter can step-up the voltage of a PV system. Figure 3 [38] shows the basic circuit configuration of a boost DC/DC power converter. An inductor (L) stores energy when the PV system power supply is turned on. Loads will receive energy from the inductor if the power supply is off.

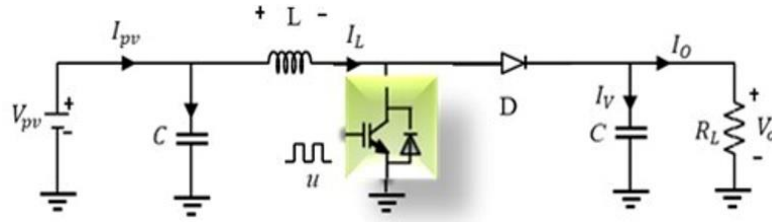


Fig. 3. Boost converter circuit

Selection of topologies: Boost converters are preferred over alternative topologies (buck-boost, Cuk, SEPIC, fly back) due to the following reasons:

1. (i) PV voltage (26.4 V) is always lower than DC bus voltage (60 V), so only step-up is required;
2. (ii) accurate maximum power point tracking (MPPT) is enabled by continuous input current;
3. (iii) 94–96% efficiency is achieved with minimal components;
4. (iv) the monotonic voltage gain (V_o/V_{in}) is simple to implement.

There are two modes of operation for converters, mode 1 and mode 2. As shown in Fig. 3(a), mode 1 operates when the transistor is ON. As shown in Fig. 3(b) [38], mode 2 starts if the transistor is off.

Figure 3(a) shows mode 1 of boost converter operation. During the OFF state, current can pass through the inductance (L) and store energy. The diode is reverse-biased to prevent current from reaching the load. Thus, the output voltage remains stable.

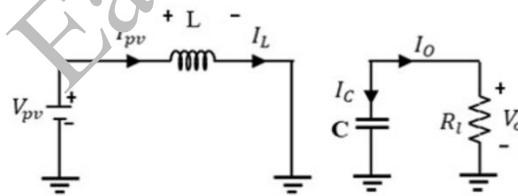


Fig. 3(a) mode 1

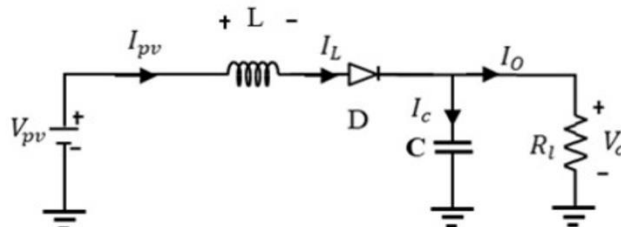


Fig. 3(b) mode 2

Figure 3(b) illustrates the operation of the boost converter in mode 2. In this mode, the transistor is off, interrupting the direct current passing through the inductance (L). By using a diode in the forward bias, the energy stored in the inductance is transferred to the load. To maintain the output voltage, the capacitor is charged, and power is supplied to the load.

The equations for the boost converter circuit are as follows (Eqs. 8–10), which serve as a component design guideline [38].

The duty cycle, S :

$$S = 1 - \frac{V_{pv}}{V_o}. \quad (8)$$

The critical value for inductance, L :

$$L = \frac{S(1-S)R_L}{2f}. \quad (9)$$

The capacitance value as a critical value, C :

$$C = \frac{S}{2fR_L}, \quad (10)$$

where: V_{pv} is the input voltage/voltage source, V_o is the average output voltage, S is the duty cycle, R_L is the resistance, f is the switching frequency, L is the inductance, and C is the capacitance.

3. Controller design

The sliding-mode control strategy is presented in this section. The fundamentals of SMC are covered in **Section 3.1**. The boost converter is modeled using an average state-space approach in **Section 3.2**. The control law is formulated in **Section 3.3**. The switching law and parameter tuning are discussed in **Section 3.4**. Robust convergence is explained intuitively in **Section 3.5**. PV modeling is linked to controller design in **Section 3.6**. Stability analysis is provided in **Section 3.7**.

3.1. Robust sliding-mode control

Robust sliding-mode control (SMC) was initially developed for linear control systems and later extended to nonlinear control systems. The algorithm design for this control method is straightforward and easy to understand, making it highly accessible for practical applications. Its effectiveness is well-documented, as it provides systems with strong anti-interference capabilities and is particularly well-suited for nonlinear applications, such as photovoltaic (PV) systems [9].

The structure of sliding-mode control is based on the principles of variable structure control systems. What sets this method apart from others is its discontinuous control nature, characterized by switching behaviors that cause the system's "structure" to change over time.

This control strategy forces the system to oscillate with small amplitude and high frequency along a predefined trajectory, a phenomenon known as sliding-mode motion or sliding-mode dynamics.

The key advantages of sliding-mode control include its simple algorithm, high reliability, and excellent robustness. These features make it an attractive choice for systems requiring stability and performance under varying conditions. The general representation of the system can be described as follows:

$$\dot{x} = f(x, u, t), x \in \mathbb{R}^n. \quad (11)$$

In the state space of $S(x) = S(x_1, x_2, \dots, x_n) = 0$, $x \in \mathbb{R}^n$, as shown in Fig. 4, the state space is divided into three regions by the surface $S = 0$, $S > 0$, and $S < 0$, respectively.

Figure 4 illustrates three distinct regions of surface switching characteristics. There are three domains within the sliding surface: $S = 0$, $S > 0$, and $S < 0$. The diagram illustrates the trajectory of the system, where the dynamics change based on the region. An equilibrium point is shown at point C on the sliding surface, while trajectories leading up to that point are shown at points A and B on the sliding surface.

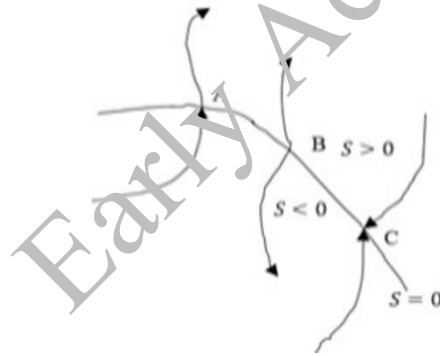


Fig. 4. Three points surface switching characteristics

By considering Fig. 4, point A is called the normal point, the system moves toward the surface $S = 0$, and finally leaves after crossing the surface; point B is called the starting point, the system leaves from the surface $S = 0$ to both sides; and point C is called the end point, the system moves from the $S > 0$ and $S < 0$ area to the surface $S = 0$. Since points of type A and B are unstable, only points of type C are meaningful. If all points in a certain area on the switching surface are type C points, when the system moves close to this range, it will be attracted to move in this area. All the endpoints in this range constitute the "sliding-mode" area. The movement of the system in this range is called sliding-mode motion. According to the characteristics of sliding-mode motion, the system moves to a position very close to the switching surface $S = 0$, and we have

$$\lim S\dot{S} \leq 0. \quad (12)$$

This condition is equivalent to the system satisfying the form

$$V(x_1, x_2, \dots, x_n) = [S(x_1, x_2, \dots, x_n)]^2. \quad (13)$$

The necessary condition of the Lyapunov function. Since the function is positive definite, and according to (13), the derivative of S^2 is semi-negative definite, it can be understood that the position V next to $S = 0$ is approximately a non-increasing function. Therefore, if Eq. (12) is met, then (13) can be used as the Lyapunov function of the system, and the system itself is stable under the condition $S = 0$. The general process of sliding-mode variable structure control can be described by the following equations.

The state equation of the system is

$$\dot{x} = f(x, u, t), \quad x \in \mathbb{R}^n, \quad u \in \mathbb{R}^m, \quad t \in \mathbb{R}. \quad (14)$$

The switching function needs to be determined:

$$S(x), S \in \mathbb{R}^m. \quad (15)$$

Solve the control function:

$$u = \begin{cases} u^+(x) & S(x) > 0 \\ u^-(x) & S(x) < 0 \end{cases} \quad (16)$$

Among them, $u^+(x) \neq u^-(x)$, so that

1. the sliding mode exists, that is, Eq. (16) holds;
2. the accessibility condition must be met, that is, the system working point must be able to approach the sliding surface reaching within the limited time;
3. the stability ensures for the sliding motion;
4. If the single-input nonlinear system $\dot{x} = f(x, u, t)$ achieves ideal sliding-mode control, it must satisfy

$$\begin{aligned} \dot{S}(x, t) &= 0, \\ \dot{S}(x, t) &= \frac{\partial S}{\partial t} f(x, u, t) + \frac{\partial S}{\partial x} \cdot \end{aligned} \quad (17)$$

Using Eq. (17), we can solve equation u , which is the average control amount of the nonlinear system on the switching surface $S = 0$. The control amount at this time is called the equivalent control amount, which is represented by u_{eq} . At this point, we can get the sliding-motion equation as follows:

$$\begin{cases} \dot{x} = f(x, u_{eq}, t) \\ S(x, t) = 0 \end{cases} \quad (18)$$

This equation represents the system moving back and forth along the sliding surface under ideal conditions. This process is carried out without external interference conditions and is an

ideal switch. This ideal situation is difficult to achieve in practice. In fact, the system will have various uncertain interference factors, and the switching frequency of the switch cannot be infinite. For these factors, the control quantity is generally equal to the equivalent control quantity plus the switching control term as the control input, as follows:

$$u = u_{eq} + u_{sw}. \quad (19)$$

Among them, the switching control term u_{sw} is to overcome possible interference and ensure that the sliding-mode arrival condition is met [9]. By using Eqs. (1)–(19), the following methodology will be realized.

3.1.1. Methodology

Based on a literature review, we present a summary of the proposed control-design approach. First, the solar model is developed by interpreting the Eqs. (1)–(7) mathematically. As part of this process, the voltage, current and power generated by the PV panel are analyzed at this stage. In addition, the inductance and capacitance of the boost converter are designed according to Eqs. (8)–(10) to ensure the desired voltage boost.

Figure 3 illustrates the state space average model of the DC/DC boost converter (20)–(22), providing a better understanding of its dynamic behavior:

$$\dot{I}_L = \frac{[V_{pv} - (1-u)V_o]}{L}, \quad (20)$$

$$\dot{I}_L = \frac{[V_{pv} - (1-u)V_o]}{L}, \quad (21)$$

$$\dot{V}_o = \frac{[-I_o + (1-u)I_L]}{C}. \quad (22)$$

Lastly, the proposed controller is developed by selecting the non-linear switching function as follows:

$$S = V_o I_L - V_{ref} I_{ref}. \quad (23)$$

To find the control law from Eq. (20), the following reach dynamics is selected.

$$\dot{S} = -[\lambda s + k \text{sgn}(s)]. \quad (24)$$

The overall control law is presented below:

$$u = \frac{-[I_o * I_L - \frac{V_{pv} * V_o}{L} - \lambda s] + k \text{sgn}(s)}{\left[\frac{(I_L)^2}{C} - \frac{(V_o)^2}{L}\right]}, \quad (25)$$

where:

$$\text{Sign}(s) = \begin{cases} 1, & S > 0 \\ 0, & S = 0 \\ -1, & S < 0 \end{cases}. \quad (26)$$

3.1.2. The switching law and the tuning of design parameters

Equation (25) has two tuning parameters: λ (proportional gain) and k (switching gain). Reachability dynamics (24) ensure convergence to the sliding surface ($S = 0$). The proportional term $-\lambda s$ determines convergence speed, while the switching term $-k \text{sgn}(s)$ compensates for disturbances and uncertainties. For faster responses, increase λ ; for better robustness, increase k ; for chattering, reduce k . With the parameters in Table 2, the controller remains stable for both λ and k .

3.1.3. A Simple explanation of robust convergence in PV systems

Appreciating the controller's effectiveness in PV applications settings requires understanding why the reachability dynamics (24) and sliding condition $S\dot{S} \leq 0$ ensure robust convergence.

1. Power-balance targets for sliding surfaces

PV has a clear physical meaning for the sliding surface (23):

- i) An output power equal to the reference power (MPP), when $S = 0$,
- ii) In the event that output power exceeds the reference level, the duty cycle must be reduced when $S > 0$,
- iii) In cases where output power is below the reference level, duty cycle must be increased.

As a result, driving directly achieves MPPT when $S < 0$.

2. Robustness is guaranteed by the sliding condition $S\dot{S} \leq 0$

$S\dot{S} \leq 0$ ensures that the squared distance to the surface, S^2 , never increases. PV systems are affected by these three factors:

- i) **Robustness of irradiance:** Even under sudden step changes ($200 \rightarrow 1000 \text{ W/m}^2$), the switching term $-k \text{sgn}(s)$ keeps moving closer to $S = 0$ in spite of the increased irradiance level.
- ii) **Robustness to temperature changes:** The MPP changes when panel temperature increases ($25^\circ\text{C} \rightarrow 75^\circ\text{C}$), but the surface $S = 0$ adapts automatically since it tracks power, not voltage or current.
- iii) **Robustness of parameters:** As long as k exceeds the magnitude of the uncertainties in R_{sh} or I_s , convergence is not affected.

3. Simplify PV illustration

Assume that a car (the PV system) is trying to stay on the center line (the sliding surface $S = 0$):

- i) When the car is far from the center, the proportional term $-\lambda s$ corrects more aggressively.
- ii) On uneven roads (irradiance variations), the switching term $-k \text{sgn}(s)$ acts as a constant force ensuring that the car always moves toward the center.
- iii) As long as the sliding condition $S\dot{S} \leq 0$ is satisfied, the car won't move further away from the center.

Despite changes in PV parameters due to temperature, aging, or manufacturing variations, the switching term remains robust. Compared to a PID controller, sliding-mode control is more effective for PV applications.

3.1.4. The interrelationship between PV modeling assumptions and controller design

The PV model presented in Section 2.1 (Eqs. (1)–(7)) describes several physical properties that directly affect the proposed sliding-mode control design. For an appreciation of the controller's performance and robustness, it is essential to understand this relationship.

- 1. Irradiance variation and photocurrent (I_{ph}):** Eq. (5) illustrates that I_{ph} scales linearly with the irradiance of G . Under real-world conditions, irradiance may vary rapidly (e.g., due to cloud passing). The sliding-mode control law in Eq. (25) compensates for these variations through the switching term $k \cdot \text{sgn}(s)$, which allows robust tracking without precise irradiance measurements.
- 2. Temperature and saturation current (I_s) effects:** Eq. (6) shows that it is strongly dependent on temperature ($\frac{T_c}{T_{ref}}$ and an exponential term). Temperature increases lead to a decrease in V_{oc} and a shift in MPP. The sliding surface (S) in Eq. (23) enforces power balance regardless of temperature-induced MPP shifts. Moreover, steady-state errors caused by variations in temperature are eliminated by the integral action of the reachability dynamics (Eq. (24)).
- 3. Shunt and series resistances (R_s, R_{sh}):** The I-V characteristic near the MPP and short-circuit regions is affected by both resistances in Eq. (4). The observations in Table 1 guide the controller design: The small R_s ensures minimal voltage drop at the MPP current ($I_{mp} = 7.58$ A), enabling efficient power extraction. As a result of the large R_{sh} , $I_{sh} = (V + IR_s)/R_{sh}$ is negligible at the MPP, simplifying the derivation of the control law without compromising accuracy.
- 4. Sliding-mode control implications:** In this case, the non-linear I-V characteristics (resulting from the exponential diode term) and uncertainties in R_s, R_{sh} motivate the selection of SMC. SMC differs from linear controllers (e.g., PID) and model-dependent methods (e.g., MPC) in the following ways:
 - i) Resistant to parameter variations (e.g., R_s varies with temperature, I_s varies with aging),
 - ii) A fast response to the sliding surface (Eq. (12) guarantees $\lim S\dot{S} \leq 0$),
 - iii) Simplicity of implementation (only two tuning parameters in Eq. 24).

Therefore, the PV modeling assumptions in Section 2.1 directly inform the controller structure in Section 3, ensuring that the proposed SMC strategy is both physically and practically feasible.

Table 1. Analyzing Luapunov stability

Steps	Stability derivation step-by-step
-------	-----------------------------------

This paper has been accepted for publication in the AEE journal. This is the version, which has not been fully edited and content may change prior to final publication.

Citation information: DOI 10.24425/ae.2026.1521

1	The Lyapunov function candidate is selected as $V = \frac{1}{2}S^2$, which is positive ($V > 0$ for $S \neq 0$) and equals zero only when the sliding surface reaches ($S = 0$).
2	The time derivative is as follows: Differentiate with respect to time: $\dot{V} = S\dot{S}$.
3	A substitute for reachability dynamics is as follows: By using $\dot{S} = -[\lambda s + k\text{sgn}(s)] \rightarrow \dot{V} = -[\lambda s + k\text{sgn}(s)] = -\lambda S^2 - k S $.
4	Analysis of signs; since $\lambda > 0$, $k > 0$, and $S^2 \geq 0$, $ S \geq 0$, we have $V \leq 0$ for all S . When $S = 0$, the derivative is zero.
5	Asymptotical stability conclusion: Asymptotically, the Lyapunov stability theorem guarantees that $V = S \rightarrow 0$. A sliding mode exists and is stable when the sliding condition $S\dot{S} \geq 0$ is satisfied.

Key considerations: PV systems assume the following assumptions: (i) uncertainty is bounded ($|\Delta(x, t)| < k$); (ii) control input is bounded ($u \in [0, 1]$). All of the PV boost converter systems in Table 2 are valid.

3.2. Stability analysis

We present a step-by-step derivation of the sliding-mode stability condition in Table 1 to make the stability analysis more accessible.

By using Eqs. (20)–(25), the proposed control algorithm is presented in Fig. 5. Figure 5 illustrates the implementation of the proposed robust sliding-mode control scheme. In the diagram, the boost converter, the PWM signal, and the sliding function control law are illustrated. Using the control equation, the photovoltaic system is stable, responds rapidly, and tracks maximum power points efficiently. Next, the result discussed will be presented.

Table 2. System parameters

Parameters name	Symbol	Value	Unit
Rated power	P_{mp}	200	W
Voltage	V_{mp}	26.4	V
Current	I_{mp}	7.58	A
Voltage open circuit	V_{op}	32.9	V
Current short circuit	I_{sc}	8.21	A
Series cells	N_s	54	-
Parallel cells	N_p	1	-
Current photo	I_{ph}	determined	A
Current short	I_{sc}	determined	A
Short circuit current of cell at 25°C and 1 000 W/m ²	I_{sc_std}	0.0032	A

This paper has been accepted for publication in the AEE journal. This is the version, which has not been fully edited and content may change prior to final publication.

Citation information: DOI 10.24425/ae.2026.1521

Operating temperature	T	25	°C
Nominal temperature	T_n	298	K
Solar irradiation	G	1 000	W/m ²
Electron charge	q	1.6e-19	C
The ideality factor of the diode	n	1.3	-
Boltzaman's constant	K	1.38e-23	J/K
Band gap energy of the semiconductor	E_{go}	1.1	eV
Series resistance	R_s	0.221	Ω
Shunt resistance	R_{sh}	415.405	Ω
Input voltage	V_{in}	2.9	V
Output voltage	V_o	60	V
Output power	P_o	200	W
Load current I_o	I_o	determined	A
Switching frequency	f_s	25 000	Hz
Duty ratio D	D	determined	-
Inductance current ripples	ΔI_L	determined	A
Voltage ripples	ΔV_o	determined	V
Converter inductance	L	determined	H
Converter capacitance, input and out	C	determined	F
Resistive load	R_L	18	Ω

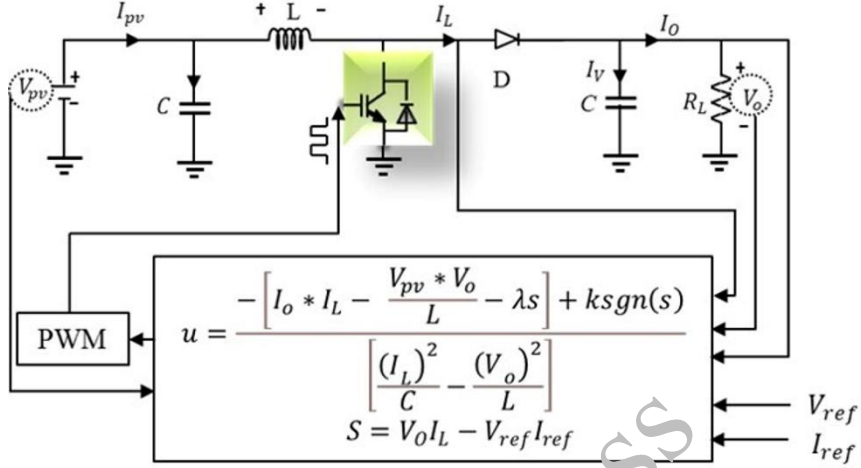


Fig. 5. Implementation of the proposed robust sliding-mode control scheme

4. Simulation results

In MATLAB/Simulink, the proposed SMC strategy is validated with a 200 W PV source, a boost converter (25 kHz switching), and the parameters listed in Table 2. The steady-state PV characteristics are examined in Section 4.1 under varying irradiance (200–1 000 W/m²) and temperature (25–75 °C), including λ and R_{sh} . In Section 4.2, dynamic performance is evaluated for nominal (0.6 mH) and perturbed (0.9 mH) converter inductance, comparing the proposed SMC with a conventional PID controller [21].

4.1. variations of parameters in (I-V) and (P-V) graphs of the PV system

This subsection examines PV steady-state characteristics under varying environmental conditions using the MATLAB/Simulink model (Table 2). We conduct two tests: irradiance variations from 200 to 1 000 W/m² at a constant 25°C. According to Figs. 6 and 7, the results of the current-voltage (I-V) and power-voltage (P-V) curves can be seen.

PV cells generally produce more power as radiation intensity increases. The rise in irradiation power is primarily driven by two factors: the short-circuit potential V_{oc} and the constant rise in irradiation current I_{ph} . Moreover, the short-circuit current I_{sc} is linearly boosted by the increase in minority carriers generated by increasing irradiation intensity, as shown in Figs. 6 and 7. Irradiance level directly affects PV cell performance. As the intensity of a radiation source increases, the series resistance R_s decreases continuously. Figures 8 and 9 show R_s decreases significantly with increasing intensity up to 200 W/m². The active layer of a solar cell's photovoltaic cell has an enhanced conductivity under higher irradiation levels, resulting in a

lower R_s . The intensity of solar radiation increases the generation of charge carriers in the material, resulting in an improvement in the overall conductivity.

A solar cell's electrical properties are directly related to the intensity of irradiation. Shunt R_{sh} behaves differently depending on irradiation intensity. At low irradiation levels around 200 W/m^2 , R_{sh} increases slightly, and at higher irradiation levels, R_{sh} increases faster. Localized inhomogeneities in the solar cell cause the initial increase in R_{sh} . These inhomogeneities are associated with defect regions with high concentrations of trapped electrons. Parallel to defect-free regions, these defect regions perform poorly. Electrical activity is greater at low current densities, especially in poor solar radiation conditions. The traps fill as irradiation intensity increases, limiting the current through the shunt and increasing R_{sh} , reaching a maximum when all traps are filled. In addition to irradiation intensity, cell heating due to high irradiance level may also degrade R_{sh} , unless other factors contribute.

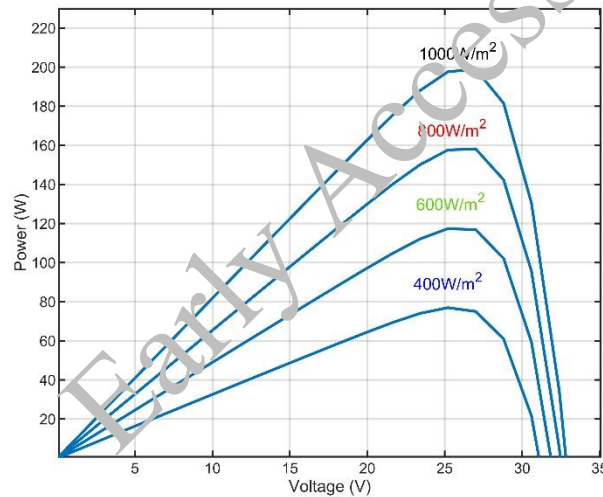


Fig. 6. Power-voltage response graphs for photovoltaic panels with various irradiances at 25°C

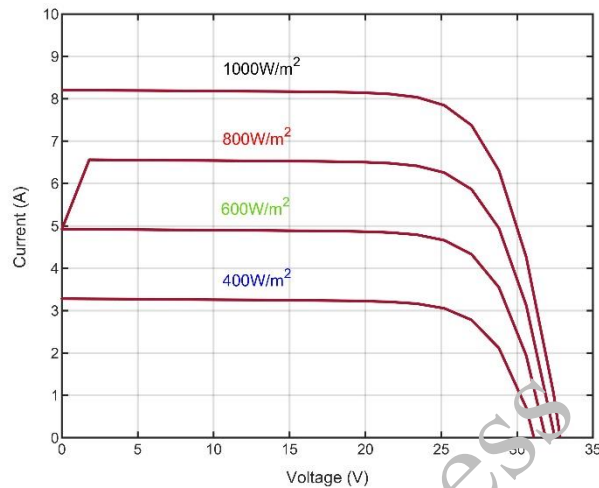


Fig. 7. Solar panel current-voltage (P-V) characteristic curves at 25°C with different irradiances

The relationship between irradiation intensity, defect dynamics, and solar cell electrical properties is complex. The shunt resistance R_{sh} in a solar cell would, in an ideal setup, be infinite, ensuring that there is no alternate path for current flow. The series resistance R_s would be zero, preventing voltage drop before the load. However, in practice, reducing the value of R_{sh} (Figs. 10 and 11) and increasing the value of R_s (Figs. 8 and 9) can adversely affect solar cell performance, affecting both the fill factor and the maximum power output P_{max} , as shown in Fig. 11.

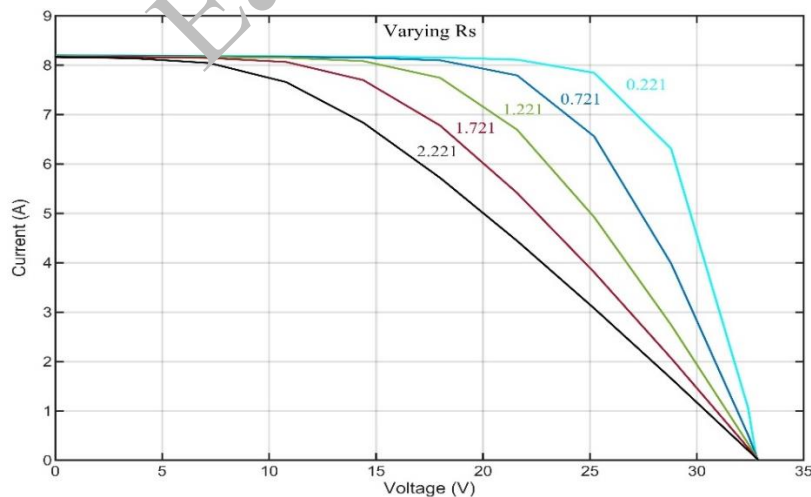


Fig. 8. The parasitic resistances of solar cells are plotted as a function of voltage levels at 25°C in order to determine their parameters

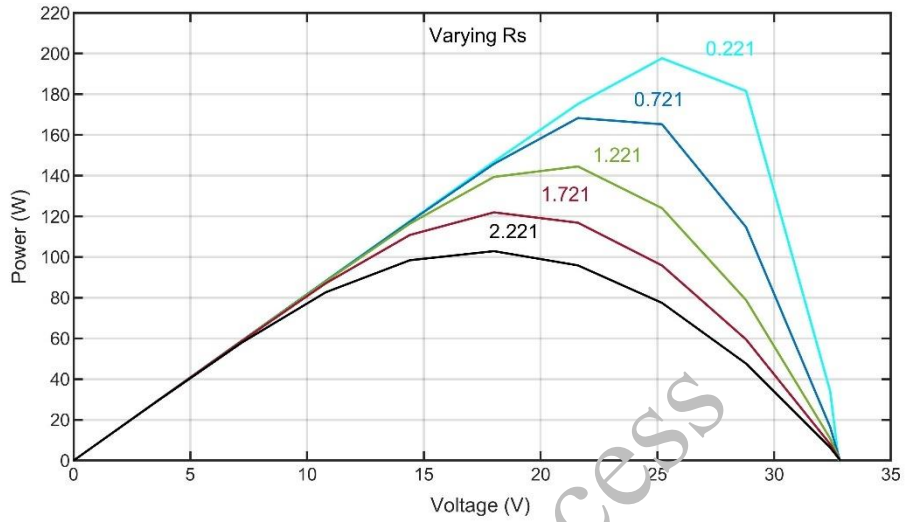


Fig. 9. At a temperature of 25°C, electrical parameters of solar cells are compared with irradiation levels

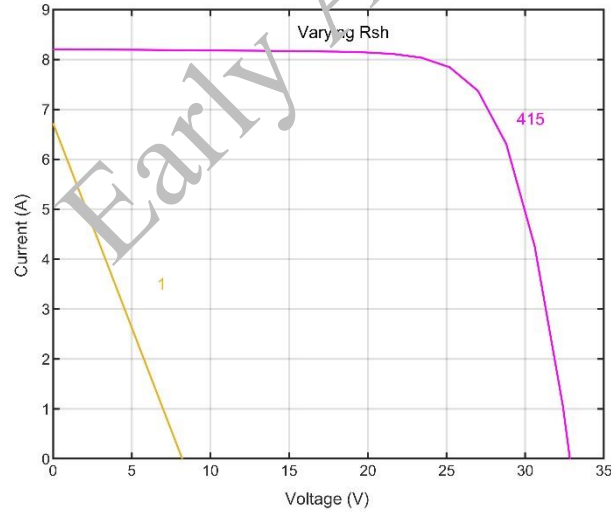


Fig. 10. The shunt resistances of solar cells are plotted as a function of voltage levels at 25°C

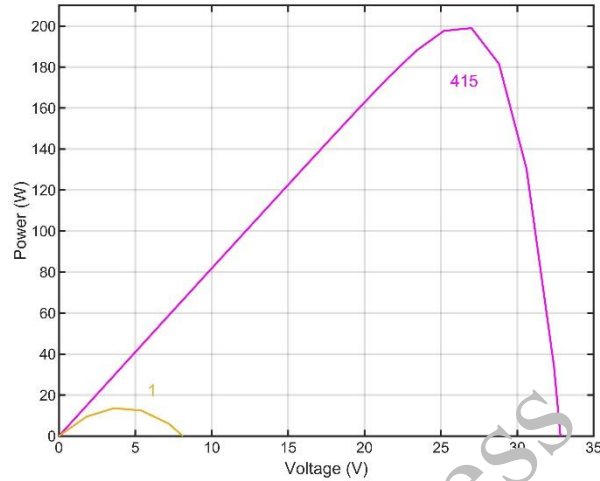


Fig. 11. The shunt resistances of solar cells are increased as a function of voltage levels at 25°C

Due to excessive leakage currents, a significant drop in V_{oc} occurs when R_{sh} is reduced excessively. A rise in internal resistance results in a decrease in short-circuit current I_{sc} , when R_s increases excessively. Schottky's formula states that I_{sc} increases linearly with irradiance level to increase photon-to-current conversion efficiency. Over time, V_{oc} increases logarithmically based on the semiconductor material's energy state distribution. P_{max} also increases with irradiation power, as shown in Fig 10. Figure 11 illustrates the relationship between R_{sh} and irradiation intensity, emphasizing that the relationship between R_s and irradiation intensity is less than one due to both inside and outside shunt resistances. Under varying irradiation conditions, it is crucial to minimize R_s and maximize R_{sh} in order to maximize R_s and R_{sh} in solar cells.

Figure 11 shows that the solar cell series resistance R_s increases with temperature. Significantly, this increase is greater on the low-temperature slope of the curve than on the high-temperature slope. As a result, R_s is temperature-dependent, and this has a substantial impact on solar cell performance. Shunt resistance R_{sh} is also crucial for maximizing solar cell efficiency. In Fig. 13, higher R_{sh} values minimize leakage currents and optimize performance. As the temperature rises (Figs. 12 and 13), R_{sh} decreases.

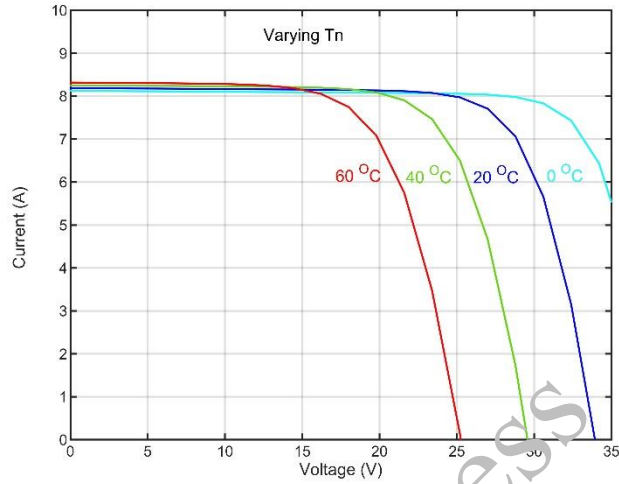


Fig. 12. A plot of the current-voltage graphs of photovoltaic cells shown in varying temperatures under the conditions of 1000 W/m^2

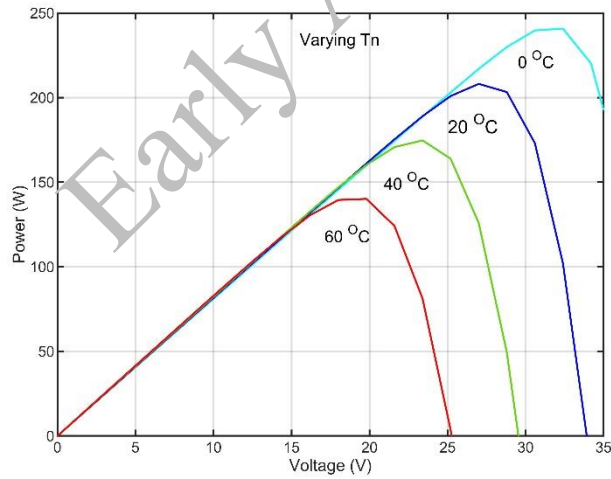


Fig. 13. A plot of the power-voltage graphs of photovoltaic cells plotted at different temperatures along with at 1000 W/m^2 .

The reduction in R_{sh} at higher temperatures further worsens the efficiency losses in photovoltaic systems. Both R_s and R_{sh} are highly temperature-dependent. As the temperature rises, R_s increases, while R_{sh} decreases. Maintaining solar cell efficiency requires proper design and temperature control.

4.2. Controller verification strategies

A comprehensive simulation framework in MATLAB/Simulink is implemented to validate the SMC strategy using the block diagram shown in Fig. 5. Using a 200 W PV source with a nominal voltage of 32 V, the DC bus voltage is regulated at 60 V by a DC/DC boost converter. All relevant system parameters, including converter components, are summarized in Table 2. The simulations were performed at different controlled ambient temperatures up to 60°C, with irradiances up to 1 000 W/m², and with a resistive load.

4.2.1. Environmental variation scenarios

Under realistic operating conditions, both stepwise and dynamic variations in solar irradiance and temperature were observed. Solar irradiance is stepped from 200 W/m² to 1 000 W/m² in order to simulate rapid changes in solar intensity caused by passing clouds. To evaluate performance, the panel temperature is increased stepwise up to 60°C. Figures 6–13 illustrate how these changes affect PV output power, voltage, and current. The figures confirm the effect of environmental factors on PV MPPT.

4.2.2. Parametric uncertainty testing

The controller's robustness is also tested against parameter uncertainties. Specifically, the boost converter's inductance is deliberately perturbed from its nominal design value of 0.6 mH to 0.9 mH. This perturbation simulates manufacturing tolerances and aging effects.

Figures 14 and 15 show transient responses under nominal and perturbed inductance conditions. Table 3 summarizes key performance metrics - overshoot, rise time, settling time, and peak time - quantitatively. Even with a 50% increase in inductance, the proposed SMC maintains fast convergence, low overshoot, and minimal transient degradation.

Table 3. Output power parametric performance metrics.

Approach	Converter inductance (mH)	Overshoot (%)	Rise time (ms)	Settling time (ms)	Peak time (ms)
Proposed approach	0.6 (nominal)	8.5	0.52	2.0	1.2
Proposed approach	0.9 (perturbed)	10.0	0.59	2.0	1.2
Approach in [21]	0.6 (nominal)	26.0	0.45	2.8	0.64
Approach in [21]	0.9 (perturbed)	33.0	0.5	3.5	0.70

4.2.3. A comparative analysis

To further demonstrate the advantages of the proposed approach, the same set of tests is repeated using a conventional PID controller [21]. In all scenarios—irradiance variations, temperature variations, and inductance perturbations—the SMC consistently outperforms the PID controller in terms of settling time and overshoot reduction. Sliding-mode controllers are

therefore inherently more robust than linear mode controllers, making them particularly suitable for island DC microgrids with dynamic operating conditions.

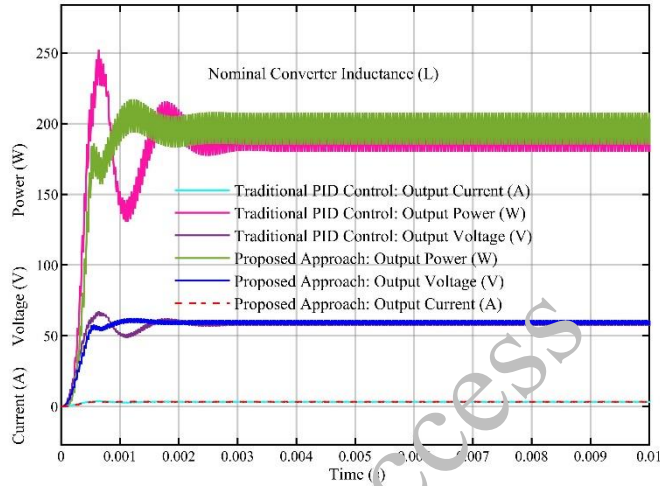


Fig. 14. Power, voltage, and current output of a PV system with nominal converter inductance (L)

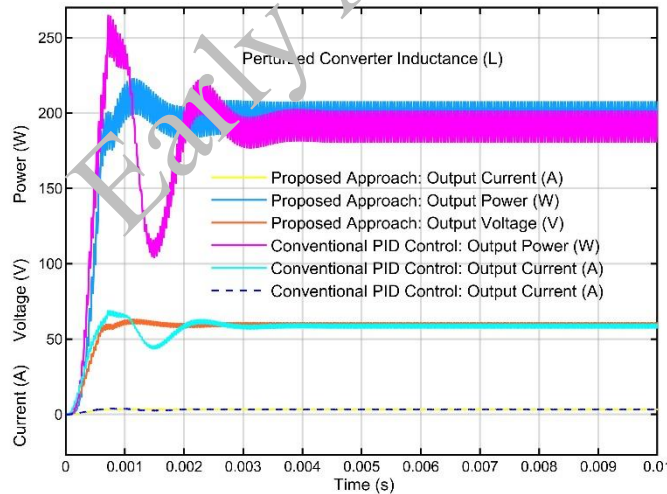


Fig. 15 Power, voltage, and current output of a PV system with perturbed converter inductance (L)

5. Conclusion

This paper proposes a robust SMC strategy to maximize power extraction from PV systems for island DC microgrid applications. We develop a mathematical model of the PV system,

This paper has been accepted for publication in the AEE journal. This is the version, which has not been fully edited and content may change prior to final publication.
Citation information: DOI 10.24425/ae.2026.1521

incorporating saturation current, shunt resistance current, and photocurrent equations. This model is developed to accurately represent its behavior under varying environmental conditions. Using a state-space approach, a DC/DC boost converter is designed and modeled, and the SMC law is formulated with a nonlinear switching function and reachability dynamics.

Based on three critical test categories in MATLAB/Simulink, the proposed control strategy was systematically validated: (i) changes in solar irradiance up to 1 000 W/m², (ii) variations in temperature up to 60°C, and (iii) parametric uncertainty (inductance perturbed from 0.6 mH to 0.9 mH). Performance metrics such as overshoot, rise time, settling time, and peak time were compared with conventional PID controllers. According to the results, the proposed SMC achieves:

- Under nominal and perturbed conditions, lower overshoot,
- Improved disturbance rejection based on faster settling time,
- Adaptability to parameter variations (e.g., inductance).

According to these findings, sliding-mode control is a highly effective, practical solution for improving PV energy conversion systems' efficiency and stability.

Future work

Based on these simulation-based results, future research will focus on:

1. The proposed SMC strategy will be experimentally validated by building a laboratory-scale PV-boost converter prototype.
2. Testing controller performance using hardware-in-the-loop (HIL) platforms (e.g., OPAL-RT, Speedgoat) under real-world irradiance and temperature profiles.
3. Implementation of the sliding-mode control strategy in field-programmable gate arrays (FPGAs).

References

- [1] Abdullahi S., Jin T., Lingom P., *Robust control strategy for inductive parametric uncertainties of DC/DC converters in islanded DC microgrid*, Journal of Modern Power Systems Clean Energy, vol. 11, no. 1, pp. 335–344 (2021), DOI: [10.35833/MPCE.2021.000241](https://doi.org/10.35833/MPCE.2021.000241).
- [2] Abdullahi S., Jin T., *Centralized controller design for voltage estimation error constrained in islanded DC-microgrids: Kalman filtering method*, Simulation Modelling Practice and Theory, vol. 125, 102753 (2023), DOI: [10.1016/j.simpat.2023.102753](https://doi.org/10.1016/j.simpat.2023.102753).
- [3] Abdullahi S., Eltag K., Weining L., Xiaohu C., *Adaptive virtual inertia and voltage estimation: enabled model predictive control for improved performance in islanded DC microgrids*, IEEE Access, vol. 13, pp. 130896–130908 (2025), DOI: [10.1109/ACCESS.2025.3591518](https://doi.org/10.1109/ACCESS.2025.3591518).
- [4] Abdullahi S., Jin T., *Improved finite control set model predictive estimation voltage control in DC-microgrids*, Electric Power Components Systems, vol. 52, no. 5, pp. 709–721 (2023), DOI: [10.1080/15325008.2023.2230960](https://doi.org/10.1080/15325008.2023.2230960).
- [5] Abdullahi S., Jin T., *Finite control set model predictive DC-grid voltage estimation control in DC-microgrids*, in IEEE Fourth International Conference on DC Microgrids (ICDCM), Arlington, VA, USA pp. 1–5 (2021), DOI: [10.1109/ICDCM50975.2021.9504660](https://doi.org/10.1109/ICDCM50975.2021.9504660).

This paper has been accepted for publication in the AEE journal. This is the version, which has not been fully edited and content may change prior to final publication.
Citation information: DOI 10.24425/ae.2026.1521

-
- [6] Awasthi A. *et al.*, *Review on sun tracking technology in solar PV system*, Energy Reports, vol. 6, pp. 392–405 (2020), DOI: [10.1016/j.egy.2020.02.004](https://doi.org/10.1016/j.egy.2020.02.004).
- [7] Islam M.A., Kabir M.A., *Neural network based maximum power point tracking of photovoltaic arrays*, TENCON 2011–2011 IEEE Region 10 Conference, Bali, Indonesia, pp. 79–82 (2011), DOI: [10.1109/TENCON.2011.6129067](https://doi.org/10.1109/TENCON.2011.6129067).
- [8] Maureira A., Riffo S., Restrepo C., González-Castaño C., Rivera M., *Model-free control of a DC–DC boost converter based on the averaging of inductor current*, Archives of Electrical Engineering, vol. 74, no. 2, pp. 487–501 (2025), DOI: [10.24425/ae.2025.153910](https://doi.org/10.24425/ae.2025.153910).
- [9] Pradhan R., Subudhi B., *Double integral sliding mode MPPT control of a photovoltaic system*, IEEE transactions on Control Systems Technology, vol. 24, no. 1, pp. 285–292 (2015), DOI: [10.1109/TCST.2015.2420674](https://doi.org/10.1109/TCST.2015.2420674).
- [10] Lasseter R.H., *Microgrids*, IEEE Power Engineering Society Winter Meeting, Conference Proceedings (Cat. No. 02CH37309), New York, NY, USA, pp. 305–308 (2002), DOI: [10.1109/PESW.2002.985003](https://doi.org/10.1109/PESW.2002.985003).
- [11] John S.S., Sony H.A., Lavanya V., Meera P.S., *Power quality improvement in microgrids using artificial intelligence techniques: A Review*, Science and Technology for Energy Transition, vol. 81, no. 14, pp. 1–21 (2026), DOI: [10.2516/stet/2026015](https://doi.org/10.2516/stet/2026015).
- [12] Gutiérrez-Escalona J., Roncero-Clemente C., Husev C., Matiushkin O., Blaabjerg F., *Artificial intelligence in the hierarchical control of AC, DC, and hybrid AC/DC microgrids: a review*, IEEE Access, vol. 12, pp. 157227–157246 (2024), DOI: [10.1109/ACCESS.2024.3486382](https://doi.org/10.1109/ACCESS.2024.3486382).
- [13] Chawda G.S., Su W., Wang M., *A comprehensive review of high-frequency AC microgrids for distribution systems*, IEEE Transactions on Smart Grid, vol. 15, no. 6, pp. 5415–5428 (2024), DOI: [10.1109/TSG.2024.3422997](https://doi.org/10.1109/TSG.2024.3422997).
- [14] Ishaq S., Khan I., Rahman S., Hussain T., Iqbal A., Elavarasan R.M., *A review on recent developments in control and optimization of micro grids*, Energy Reports, vol. 8, pp. 4085–4103 (2022), DOI: [10.1016/j.egy.2022.01.080](https://doi.org/10.1016/j.egy.2022.01.080).
- [15] Tomás-Martín A., Kuznetsov B., García-Cerrada A., Sigrist L., Bueno E.J., *Decentralised consensus-based hierarchical control of a hybrid AC–DC microgrid robust to communication delays*, International Journal of Electrical Power Energy Systems, vol. 175, pp. 111645 (2026), DOI: [10.1016/j.ijepes.2026.111645](https://doi.org/10.1016/j.ijepes.2026.111645).
- [16] Elkholy M., Yona A., Ueda S., Said T., Senjyu T., Lotfy M.E., *Experimental investigation of AI-enhanced FPGA-based optimal management and control of an isolated microgrid*, IEEE Transactions on Transportation Electrification, vol. 10, no. 2, pp. 3670–3679 (2023), DOI: [10.1109/TTE.2023.3315729](https://doi.org/10.1109/TTE.2023.3315729).
- [17] Huang S. *et al.*, *Hierarchical robustness strategy combining model-free prediction and fixed-time control for islanded AC microgrids*, IEEE Transactions on Smart Grid, pp. 4380–4394 (2025), DOI: [10.1109/TSG.2025.3591597](https://doi.org/10.1109/TSG.2025.3591597).
- [18] Yang T., Lai J., Yu C., Wang X., Xiao Q., *Distributed two-layer predictive control of AC microgrid clusters with communication delays*, IEEE Transactions on Smart Grid, vol. 16, no. 3, pp. 2040–2051 (2025), DOI: [10.1109/TSG.2025.3539789](https://doi.org/10.1109/TSG.2025.3539789).
- [19] Gao J., Gao D., Xiao C., *Multi-Time Scale Coordinated Optimization of Energy Systems Under Flexible Load Response*, HighTech and Innovation Journal, vol. 6, no. 2, pp. 384–397 (2025), DOI: [10.28991/HIJ-2025-06-02-02](https://doi.org/10.28991/HIJ-2025-06-02-02).

This paper has been accepted for publication in the AEE journal. This is the version, which has not been fully edited and content may change prior to final publication.

Citation information: DOI 10.24425/ae.2026.1521

-
- [20] Naidu I., Padmavathi T., Padmavathi S.V., Kumar B.U., *Intelligence based controlling models for effective power tracking and voltage enhancement in grid-pv systems*, Emerging Science Journal, vol. 9, no. 1, pp. 261–283 (2025), DOI: [10.28991/ESJ-2025-09-01-015](https://doi.org/10.28991/ESJ-2025-09-01-015).
- [21] Ma'arif A., Nugraha I., Maghfiroh H., Furizal F., Suwarno I., *DC Motor Angular Speed Controller Using an Embedded Microcontroller-Based PID Controller*, Emerging Science Journal, vol. 9, no. 6, pp. 2915–2928 (2025), DOI: [10.28991/ESJ-2025-09-06-03](https://doi.org/10.28991/ESJ-2025-09-06-03).
- [22] Zhang Y., Świdorski K., Xu Q., *A Dynamic Power Management Strategy for Cascaded Multilevel Converter with Hybrid Energy Storage System*, IEEE Transactions on Industrial Electronics, vol. 72, no. 12, pp. 13253–13263 (2025), DOI: [10.1109/TIE.2025.3579091](https://doi.org/10.1109/TIE.2025.3579091).
- [23] Muthukumar P., Venkateshkumar M., Chin C.S., *A comparative study of cutting-edge bi-directional power converters and intelligent control methodologies for advanced electric mobility*, IEEE Access, vol. 12, pp. 28710–28752 (2024), DOI: [10.1109/ACCESS.2024.3360267](https://doi.org/10.1109/ACCESS.2024.3360267).
- [24] Adiche S. *et al.*, *Advanced control strategy for AC microgrids: a hybrid ANN-based adaptive PI controller with droop control and virtual impedance technique*, Scientific Reports, vol. 14, no. 1, 31057 (2024), DOI: [10.1038/s41598-024-82193-1](https://doi.org/10.1038/s41598-024-82193-1).
- [25] Tang H.H., Ahmad N.S., *Fuzzy logic approach for controlling uncertain and nonlinear systems: a comprehensive review of applications and advances*, Systems Science Control Engineering, vol. 12, no. 1, 2394429 (2024), DOI: [10.1080/21642583.2024.2294429](https://doi.org/10.1080/21642583.2024.2294429).
- [26] Shenbagalakshmi R., Mittal S.K., Subramaniam J., Venkatesan V., Manikandan D., Ramaswamy K., *Adaptive speed control of BLDC motors for enhanced electric vehicle performance using fuzzy logic*, Scientific Reports, vol. 15, no. 1, 12579 (2025), DOI: [10.1038/s41598-025-90957-6](https://doi.org/10.1038/s41598-025-90957-6).
- [27] Guo Q., Bahri I., Diallo D., Berthelot E., *Model predictive control and linear control of DC–DC boost converter in low voltage DC microgrid: An experimental comparative study*, Control Engineering Practice, vol. 131, 105387 (2023), DOI: [10.1016/j.conengprac.2022.105387](https://doi.org/10.1016/j.conengprac.2022.105387).
- [28] Mardani M.M., Khooban M.H., Mahmoudian A., Dragičević T., *Model predictive control of DC–DC converters to mitigate the effects of pulsed power loads in naval DC microgrids*, IEEE Transactions on Industrial Electronics, vol. 66, no. 7, pp. 5676–5685 (2018), DOI: [10.1109/TIE.2018.2877191](https://doi.org/10.1109/TIE.2018.2877191).
- [29] Li Y., Sahoo S., Dragičević T., Zhang Y., Blaabjerg F., *Stability-oriented design of model predictive control for DC/DC boost converter*, IEEE Transactions on Industrial Electronics, vol. 71, no. 1, pp. 922–932 (2023), DOI: [10.1109/TIE.2023.3247785](https://doi.org/10.1109/TIE.2023.3247785).
- [30] Ghosh S.K., Roy T.K., Alam Z., Saha S., Alzahrani A., *Transient stability enhancement of DC–DC boost converters feeding constant power loads in DC microgrid applications via composite nonlinear control techniques*, IEEE Access, vol. 11, pp. 69951–69964 (2023), DOI: [10.1109/ACCESS.2023.3291772](https://doi.org/10.1109/ACCESS.2023.3291772).
- [31] Mahmud M.R., Pota H., *Robust feedback linearizing controller design for dc microgrid connected dc-dc converter*, IEEE Texas Power and Energy Conference (TPEC), College Station, TX, USA, pp. 1–6 (2021), DOI: [10.1109/TPEC51183.2021.9384979](https://doi.org/10.1109/TPEC51183.2021.9384979).
- [32] Wang F., Zhou C., Hua C., Systems C., *Dynamic observer-based fast fixed-time filtered backstepping controller design for a constrained uncertain nonlinear system*, IEEE Transactions on Systems, vol. 53, no. 6, pp. 3640–3653 (2023), DOI: [10.1109/TSMC.2022.3230429](https://doi.org/10.1109/TSMC.2022.3230429).
- [33] Melath G., Hussain M.N., Agarwal V., *A nonlinear adaptive backstepping controller for stabilizing the DC bus voltage of an islanded hybrid microgrid*, IEEE Journal of Emerging Selected Topics in Industrial Electronics, vol. 3, no. 3, pp. 538–548 (2022), DOI: [10.1109/JESTIE.2022.3160666](https://doi.org/10.1109/JESTIE.2022.3160666).

This paper has been accepted for publication in the AEE journal. This is the version, which has not been fully edited and content may change prior to final publication.

Citation information: DOI 10.24425/ae.2026.1521

-
- [34] Sami I., Salman M., Koh H.-G., Boccaletti C., Al-Ismail F.S., *Barrier Adaptive Nonlinear Finite Time Control Strategy for Resilient Voltage Stabilization in DC Microgrids*, IEEE Open Journal of Industry Applications, vol. 7, pp. 174–190 (2026), DOI: [10.1109/OJIA.2026.3658248](https://doi.org/10.1109/OJIA.2026.3658248).
- [35] Razaque A. *et al.*, *Optimizing Internet-of-Things Energy Management: Integrating Theory of Inventive Problem Solving with Transfer Learning and Advanced Optimization Algorithms*, IEEE Access, vol. 13, pp. 142651–142673 (2025) DOI: [10.1109/ACCESS.2025.3590050](https://doi.org/10.1109/ACCESS.2025.3590050).
- [36] Islam M.S., Bushra I.J., Roy T.K., Oo A.M.T., *Virtual capacitor-based robust composite controller for stability enhancement in DC microgrids with wind, PV and battery integration*, IET Generation, Transmission, and Distribution, vol. 19, no. 1, e70125 (2025), DOI: [10.1049/gtd2.70125](https://doi.org/10.1049/gtd2.70125).
- [37] Twaisan K., Barışçı N., *Integrated distributed energy resources (DER) and microgrids: modeling and optimization of DERs*, Electronics, vol. 11, no. 18, 2816 (2022), DOI: [10.3390/electronics11182816](https://doi.org/10.3390/electronics11182816).
- [38] Firdaus A.A., Normahira M., Syahirah K., Sakinah J., *Design and simulation of Fuzzy Logic Controller for boost converter in renewable energy application*, in IEEE International Conference on Control System, Computing and Engineering, Penang, Malaysia, pp. 520–524 (2013), DOI: [10.1109/ICCSCE.2013.6720020](https://doi.org/10.1109/ICCSCE.2013.6720020).